Impact of nucleation conditions on the structural and optical properties of *M*-plane GaN($1\bar{1}00$) grown on γ-$LiAlO_2$

Yue Jun Sun,[a] Oliver Brandt, Uwe Jahn, Tian Yu Liu, Achim Trampert, Sven Cronenberg, Subhabrata Dhar, and Klaus H. Ploog
Paul-Drude-Institut für Festkörperelektronik, Hausvogteiplatz 5-7, D-10117 Berlin, Germany

(Received 10 July 2002; accepted 20 August 2002)

We investigate the structural and optical properties of *M*-plane GaN($1\bar{1}00$) films grown on $LiAlO_2$(100) with nucleation layers grown at high and low temperatures. Samples with a high temperature nucleation layer are found to exhibit a highly anisotropic surface morphology with pronounced corrugation, which basically replicates the surface morphology of the substrate. Photoluminescence spectra of these layers are dominated by a transition at 3.356 eV, which is absent for samples with a low-temperature nucleation layer. In conjunction with scanning electron microscopy, cathodoluminescence maps reveal that this transition predominantly stems from regions below the trenches of the surface corrugation. Transmission electron microscopy shows an abundance of stacking faults within these regions. Excitation-dependent and time-resolved photoluminescence demonstrates the intrinsic character of the 3.356 eV emission, which is thus attributed to excitons bound to stacking faults acting as ultrathin vertical quantum wells in these samples. Low-temperature nucleation is imperative to avoid thermal roughening of the substrate and thus the formation of a high density of stacking faults. © *2002 American Institute of Physics.* [DOI: 10.1063/1.1513874]

I. INTRODUCTION

γ-$LiAlO_2$ (LAO) has a tetragonal structure with lattice constants $a=b=0.5169$ nm and $c=0.6268$ nm. The LAO(100) plane exhibits a comparatively small lattice mismatch to GaN($1\bar{1}00$) (the *M* plane), namely $[0001]_{GaN}\|[010]_{LAO}\sim 0.3\%$ and $[11\bar{2}0]_{GaN}\|[001]_{LAO}\sim 1.7\%$. The GaN($1\bar{1}00$) plane is nonpolar since it is composed of equal numbers of threefold coordinated Ga and N atoms. Furthermore, GaN is not piezoelectrically active along the $[1\bar{1}00]$ direction. The resulting absence of electrostatic fields in this direction constitutes a distinct advantage for fabricating high-efficiency GaN-based light emitting diodes (LEDs) over corresponding [0001]-oriented structures on conventional substrates such as Al_2O_3(0001) and SiC(0001), the performance of which is degraded by the presence of both spontaneous and piezoelectric polarization along the growth direction.[1] In addition, LAO can be selectively etched with respect to the GaN epilayers, allowing the fabrication of on-chip LEDs.

Despite these potential advantages, LAO has been rarely used as a substrate for GaN growth.[2] We have recently reported the growth of pure *M*-plane GaN on LAO(100)[1] and have studied the fundamental optical properties of this material,[3,4] but a systematic investigation of the impact of the growth conditions on the properties of the GaN epilayers is still lacking.

In our study of this issue, we first found that pure *M*-plane layers are obtained exclusively on a particular face of LAO(100). While we cannot yet provide microscopic identification of this face, it may phenomenologically be identified by the fact that it is not attacked by 30 min exposure to HCl (32%) at 60 °C, which induces visible roughening of the opposite face. Second, we found that N-rich nucleation conditions invariably induce a phase mixture, regardless of the substrate face. Investigations of these phase-mixed films are hampered by the fact that they tend to peel off the substrate, indicating the weak interfacial bonds between *C*-plane GaN and LAO(100). In this article, we thus focus on pure *M*-plane GaN layers grown under identical conditions, except for the nucleation temperature. The layers are shown to exhibit distinctly different optical properties. We found that this effect is linked to the generation of stacking faults at high nucleation temperature, and is most likely due to thermal roughening of the substrate.

II. EXPERIMENT

In the following, we discuss the properties of two GaN($1\bar{1}00$) layers grown on LAO(100) substrates by plasma-assisted molecular beam epitaxy (PAMBE). The system is equipped with reflection high-energy electron diffraction (RHEED) for monitoring the growth. The as-received substrates are degreased with organic solvents and dipped briefly (30 s) in de-ionized (DI) water (H_2O). Next, the LAO substrate is soldered onto a Si substrate with In, which is then clipped to a Mo holder. Prior to growth, the substrate is outgassed in a load-lock chamber for 1 h at 200 °C. During the growth of sample A, both the substrate temperature (about 750 °C) and N_2 flux are kept constant during the whole growth run. The thickness of this film is 500 nm.

[a]Electronic mail: yjsun@pdi-berlin.de

 © 2002 American Institute of Physics

Downloaded 18 Jun 2004 to 62.141.165.57. Redistribution subject to AIP license or copyright, see http://jap.aip.org/jap/copyright.jsp

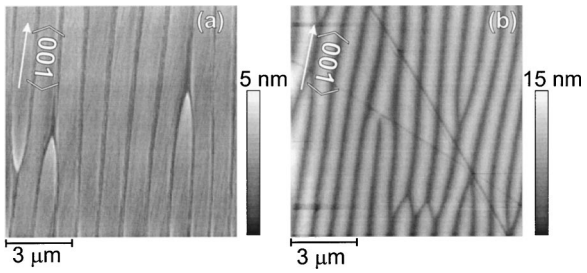

FIG. 1. $10\times10\ \mu m^2$ AFM micrographs of the surface of a typical as-received LAO(100) substrate (a) and after heating in vacuum to 750 °C (b).

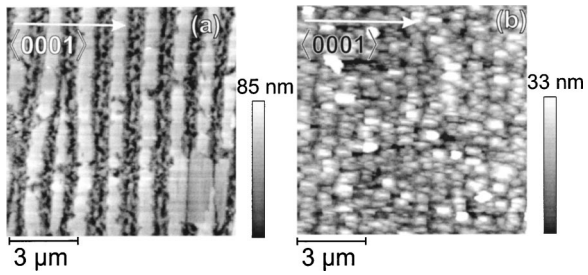

FIG. 2. $10\times10\ \mu m^2$ AFM micrographs of the surfaces of two *M*-plane GaN films: sample A (a) and sample B (b).

Sample B is nucleated first at 660 °C for the first 100 nm and then grown at 750 °C for the remaining 400 nm, using the same N_2 flux as that of sample A.

The samples are characterized by x-ray diffraction (XRD), atomic force microscope (AFM), transmission electron microscopy (TEM), continuous wave (cw)- and time-resolved photoluminescence (PL), cathodoluminescence (CL) and scanning electron microscopy (SEM). Symmetric x-ray ω–2θ scans are taken with a Bede D3 high resolution triple-crystal diffractometer with a Bartels-type Ge(022) monochromator and a Si(111) analyzer, utilizing Cu $K\alpha_1$ radiation with a wavelength of 0.154 0562 nm. The layer morphology is studied with a Park Scientific Instruments AFM system. Continuous wave PL spectra at various temperatures and excitation intensities are recorded using the 325 nm line of a He–Cd laser. Time-resolved PL measurements at 5 K are done with a frequency-tripled Ti:sapphire laser with a pulse width of about 200 fs. For detection, a Hamamatsu C5680 streak camera is used. TEM studies are performed in a JEOL3010 microscope operating at 300 kV. CL measurements are performed at 5 K in a scanning electron microscope equipped with an Oxford mono-CL2 and He-cooling stage. Surface micrographs are obtained by the same SEM at room temperature (unless otherwise specified). The generation rate is varied by changing the excitation area, but keeping the acceleration voltage (4 kV) and beam current (0.3 nA) constant. Its value is calculated taking backscattering corrections into account.

III. RESULTS AND DISCUSSION

Despite the potential merits of LAO as a promising substrate for GaN mentioned above, it also possesses a number of drawbacks which one should bear in mind. For instance, LAO is inhomogeneously etched by a variety of acids, making substrate preparation an intricate task. Worse, LAO is hydrolytic,[5] and care must be taken to limit the exposure to H_2O to a brief dip. Furthermore, LAO is thermally much less stable than, for example, Al_2O_3 or SiC, despite its high melting point of about 1700 °C.[6] Lee *et al.*[7] pointed out that the dissociation of LAO at a typical metalorganic chemical vapor deposition (MOCVD) growth temperature of ~1040 °C might restrict its use to the MBE technique and indeed the incongruent evaporation of Li_2O occurs at high temperature.[8]

Figure 1(a) shows the typical surface morphology of an as-received LAO(100) substrate. While its surface is quite smooth as indicated from the peak-to-valley (P/V) roughness of 5 nm and an root mean square (rms) roughness of 0.6 nm, a periodic trench pattern is clearly observed. The RHEED pattern observed from this substrate once it is transferred to the MBE system is a dim, streaky (1×1). However, upon heating the substrate to our standard growth temperature of 750 °C in vacuum, the pattern degrades and exhibits transmission features. In fact, as can be seen in Fig. 1(b), the corrugation of the surface has increased significantly, suggesting that LAO starts to decompose even at our comparatively low growth temperature. *Ex situ* rapid thermal annealing in nitrogen ambient at various temperatures shows a linear increase of the corrugation depth with the annealing temperature.

The growth of both samples A and B is initiated directly after igniting the N plasma. Once growth is started, the RHEED pattern initially vanishes, and a clear *M*-plane GaN pattern, consisting of superposition of streaks and facet chevrons, is then observed after 10 nm of deposition. The facets gradually diminish upon further growth.

A. Morphology and phase purity

The surface morphologies of the two samples under investigation are shown in Fig. 2. Sample A exhibits a highly periodic trench-like pattern with pronounced corrugation. Smooth elongated plateaux with a P/V roughness of ~3 nm and a rms roughness of ~0.4 nm are separated by significantly rougher trenches. The orientation of these stripes is investigated by Raman scattering and is found to be along $\langle 11\bar{2}0\rangle$, i.e., perpendicular to the *c* axis. Since the orientation relationship of *M*-plane GaN and LAO is $[11\bar{2}0]_{GaN}\|[001]_{LAO}$, the trenches run along the same direction as those observed in the substrate. It thus appears that the GaN morphology basically replicates that of the substrate. In contrast, sample B exhibits a significantly smoother and less anisotropic surface morphology, although some preferential alignment can still be observed.

To examine the phase composition of the two samples, we utilize high-resolution x-ray diffraction scans. Figure 3 presents ω–2θ scans of both samples. The peaks located at $2\theta=34.682°$ and ~32.254° are due to the (200) and $(1\bar{1}00)$ reflections of LAO and GaN, respectively. No peak related to the (0002) *C* phase is detected, which, if present, should be seen in the vicinity of the left LAO(200) diffraction peak, namely, at $2\theta=34.56°$. The values of the angular separation between these two peaks indicate lattice expansion of 0.63% and 0.70% along the $[1\bar{1}00]$ growth direction of samples A and B, respectively. This expansion is a consequence of the

Downloaded 18 Jun 2004 to 62.141.165.57. Redistribution subject to AIP license or copyright, see http://jap.aip.org/jap/copyright.jsp

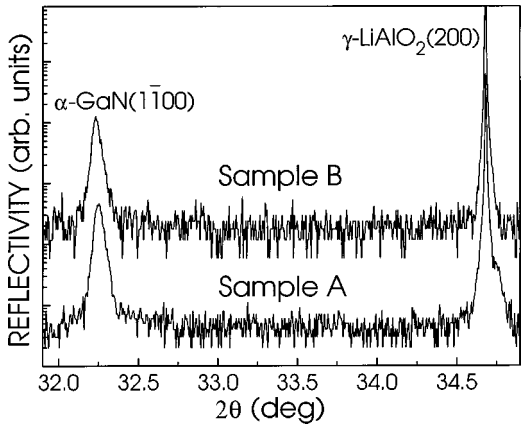

FIG. 3. ω–2θ triple crystal scans across the (1$\bar{1}$00) GaN reflection of samples A and B.

thermal and/or the lattice mismatch between GaN and LAO, both of which result in compressive in-plane strain.

XRD rocking curves of these two samples exhibit a width of 1020 arsec for sample A and 780 arcsec for sample B. As we will see below, the reduced out-of-plane orientational spread for sample B is in fact related to a reduced density of structural defects, although the actual difference between samples A and B is more dramatic than what is reflected by the rocking curves.

B. Correlation of optical and structural properties

Figure 4 shows PL spectra of samples A and B at 5 K. The PL spectra of both samples are dominated by strong near-band-gap transitions. Yellow luminescence (YL) is undetectable in either sample. The high energy band-edge lines near 3.48 eV of both samples are attributed to the donor bound exciton (D^0,X). The blueshift of the (D^0,X) transition compared to that of relaxed GaN (Refs. 9 and 10) provide evidence of the comparatively large compressive stress in the layers, consistent with the XRD result. In addition to the (D^0,X) transitions, the spectra of both samples exhibit a lower-energy line at 3.356 eV for sample A (X) and at 3.30 eV for sample B. Considering the large compressive strain in these layers, at least the latter of these lines is suspiciously

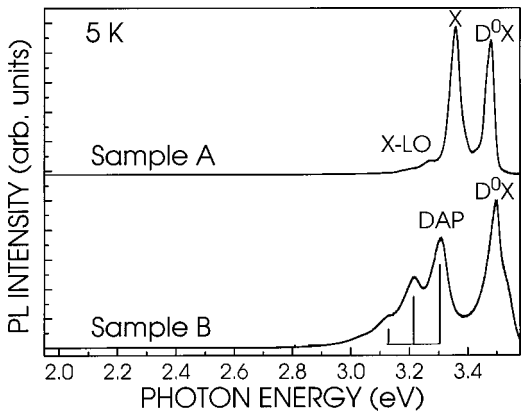

FIG. 4. Photoluminescence spectra of samples A and B recorded at 5 K. The equidistant phonon replicas are indicated by vertical lines.

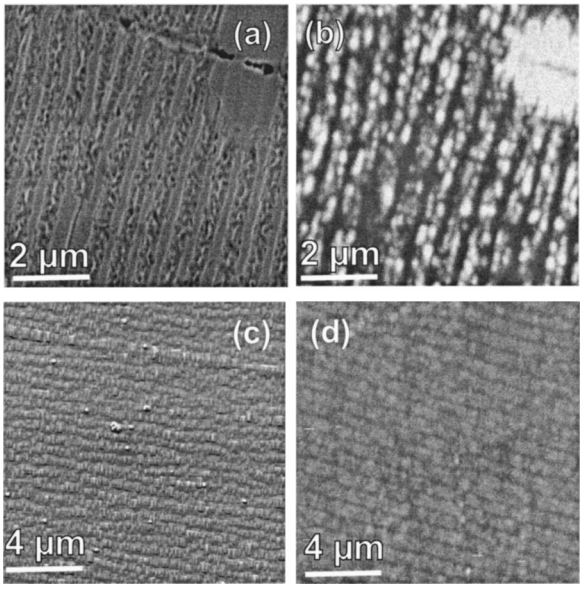

FIG. 5. Room-temperature plane-view SEM micrograph of sample A (a) and a CL map obtained from the same region at 5 K, detected at the wavelength of the X line (b); room-temperature plane-view SEM micrograph of sample B (c) and a CL map at 5 K, detected at the wavelength of the DAP line (d).

close to the position of the donor-to-acceptor pair (DAP) transition.[11–13] With regard to the former line, several groups have reported a weak PL line around 3.36 eV at low temperatures from C-plane GaN samples grown by different techniques and on different substrates,[14–20] and have mostly attributed this transition to excitons bound to structural defects, such as stacking faults[18] or dislocations.[15–17] In the following, we investigate the origin of the low-energy lines of samples A and B in detail.

Since we expect a transition related to structural defects to exhibit a larger degree of spatial inhomogeneity than a transition arising from point defects, we first perform spatially resolved CL measurements. Figure 5(a) shows a plan-view SEM image of sample A at room temperature. As in the AFM image of Fig. 2(a), we observe a stripe-like pattern consisting of rather smooth ridges and rough trenches. The CL map at the wavelength of the X line recorded at 5 K is shown in Fig. 5(b). The emission does indeed preferentially occur along the stripe direction. The superposition of the SEM and CL map (not shown here) demonstrates that the X line predominantly originates from the trench regions. For comparison, we show SEM and CL maps of sample B in Figs. 5(c) and 5(d), respectively. Evidently, the DAP emission from sample B is significantly more uniform compared to the X emission from sample A shown in Fig. 5(b). Still, it is not entirely uniform, and seems to occur preferentially on the ridges.

For sample A, the higher light-extraction efficiency in the rough trenches compared to the smooth ridges might facilitate stronger external emission intensity, causing spurious contrast in the CL map. However, as seen in the cross-sectional SEM and CL micrographs shown in Figs. 6(a) and 6(b), respectively, the X line emission actually occurs within the entire depth of layer, and not preferentially from the surface. For sample B, in contrast, we believe that the plate-like

Downloaded 18 Jun 2004 to 62.141.165.57. Redistribution subject to AIP license or copyright, see http://jap.aip.org/jap/copyright.jsp

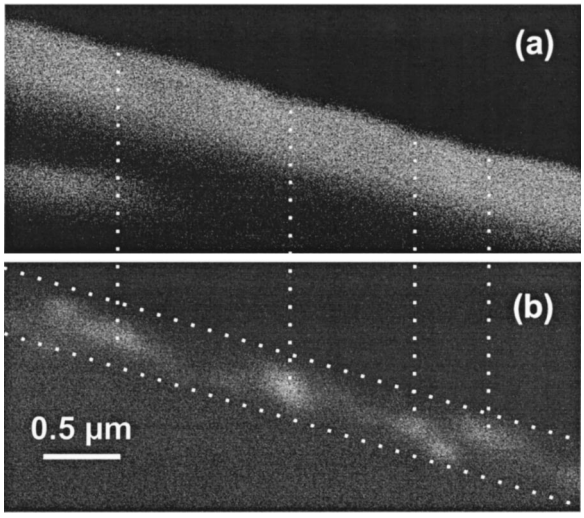

FIG. 6. Cross-sectional SEM micrograph recorded at 5 K (a) and the corresponding CL map of the same region, detected at the wavelength of the *X* line (b) of sample A.

morphology of the ridges actually enhances light extraction, since we do observe the same apparent contrast also when recording CL maps at the wavelength of the (D^0,X) transition.

To examine the microstructure of the layers, we employ cross-sectional TEM. Figure 7 shows two-beam bright field micrographs of cross sections of samples A and B with $\mathbf{g}=1\bar{1}00$ near the $[11\bar{2}0]$ zone axis. The microstructure of both samples is quite different from that of *C*-plane GaN. The density of perfect threading dislocations is found to be

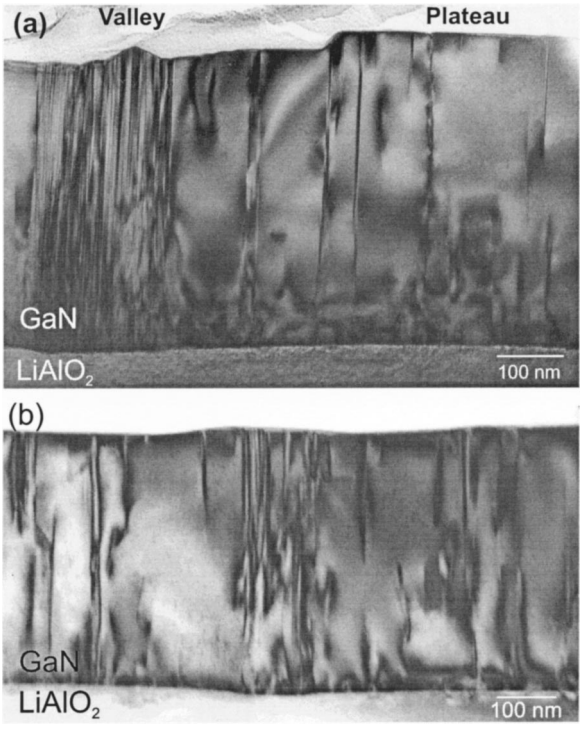

FIG. 7. Cross-sectional $\mathbf{g}=1\bar{1}00$ two-beam bright-field TEM micrographs near the $[11\bar{2}0]$ zone axis of sample A (a) and sample B (b). The defects running through the layers are identified as basal plane stacking faults.

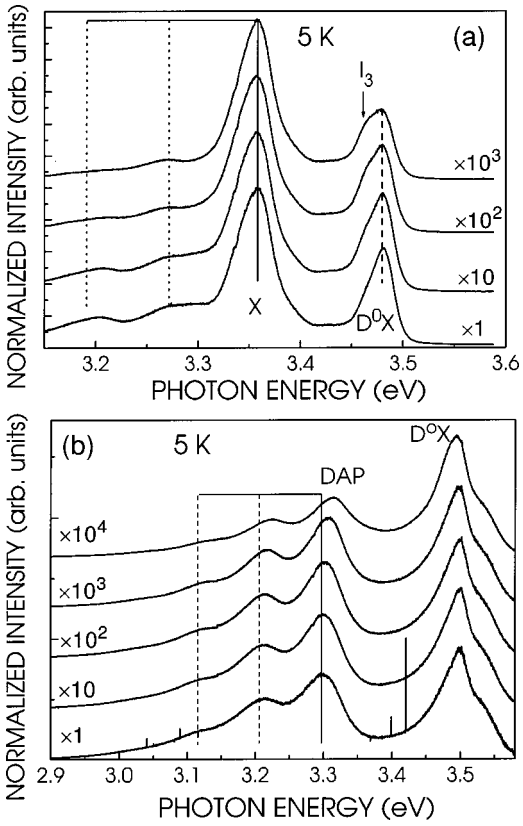

FIG. 8. Excitation density-dependent PL spectra of sample A (a) and sample B (b) at a fixed temperature of 5 K. The unit generation rate in (a) and (b) is 9×10^{15} and 8.35×10^{15} cm^{-2} s^{-1}, respectively. The equidistant phonon replicas are indicated by vertical lines.

lower than 8×10^8 cm^{-2}. The most dominant defects are basal plane stacking faults (SFs), most of which intersect the entire thickness of the layer. The partial dislocations terminating these basal plane SFs have been determined to be of Shockley type with Burgers vectors $\mathbf{b}=\frac{1}{3}[10\bar{1}0]$ or $\frac{1}{3}[01\bar{1}0]$.[21] Most important, sample A exhibits a significantly higher SF density compared to sample B, and most of the SFs in this sample are concentrated within the trench region.

It is interesting to note that in both samples bundles of SFs occur at locations where the substrate/epilayer interface is visibly disturbed. It is thus likely that the abundance of SFs in sample A results from the pronounced roughening of the LAO(100) face when heated to the growth temperature. At the same time, the high nucleation temperature used for sample A may also facilitate enhanced incorporation of O during the initial stage of growth, or even the formation of interfacial polytypoids of type (Ga,Al)(N,O). In fact, Hagege *et al.*[22–24] suggested that the presence of O may serve to stabilize SFs in AlN ceramics. We are, at present, unable to distinguish between these two possibilities, but it is clear that in both cases a low nucleation temperature results in a significantly improved microstructure and surface morphology. Furthermore, it is also clear that the *X* emission from sample A is in fact related to the presence of SFs, since the emission is strongest at places where the SFs are most abundant.

Downloaded 18 Jun 2004 to 62.141.165.57. Redistribution subject to AIP license or copyright, see http://jap.aip.org/jap/copyright.jsp

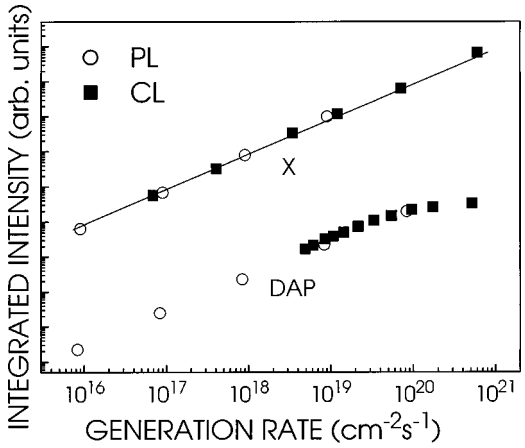

FIG. 9. Integrated PL and CL intensity of the low energy bands in sample A (*X*) and B (DAP) vs the generation rate. The solid line is a linear fit with a slope of 1.0. The experimental data for PL and CL are vertically offset for clarity.

C. Optical properties: Excitation-density dependence and recombination dynamics

Having established the correlation between the presence of SFs and the *X* emission, the question remains whether this emission merely originates from point defects and impurities which are accumulated in the vicinity of the SFs, or is in some sense an emission intrinsic to SFs, e.g., excitons bound to SFs. For this, we investigate the dependence of the low-energy PL lines from samples A and B on excitation density, as well as the recombination dynamics of these transitions.

Figures 8(a) and 8(b) show the excitation-density-dependent PL spectra of samples A and B, respectively, at 5 K in the near-band gap spectral region. For better comparison with the CL measurements given below, the excitation density is given in units of generation rate per unit area, which is identical to the photon flux in the case of PL. For sample A, the position and width of the *X* line are independent of the generation rate. In contrast, the DAP line of sample B exhibits a clear blueshift with an increase in generation rate, which is a signature of DAP transitions because of the saturation of long-distance DAPs with increasing carrier density. For both samples, the (D^0,X) transition energy is, as expected, independent of the generation rate. The low-energy shoulder (labeled I_3) of the (D^0,X) transition in sample A has an energy separation of 19 meV and thus may originate from an acceptor-bound exciton or a donor-to-band transition.

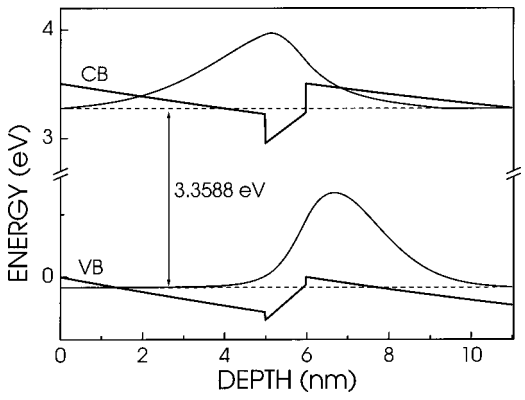

FIG. 10. Band profile, energy states, and electron-hole wave functions of a type II SF in a wurtzite GaN matrix.

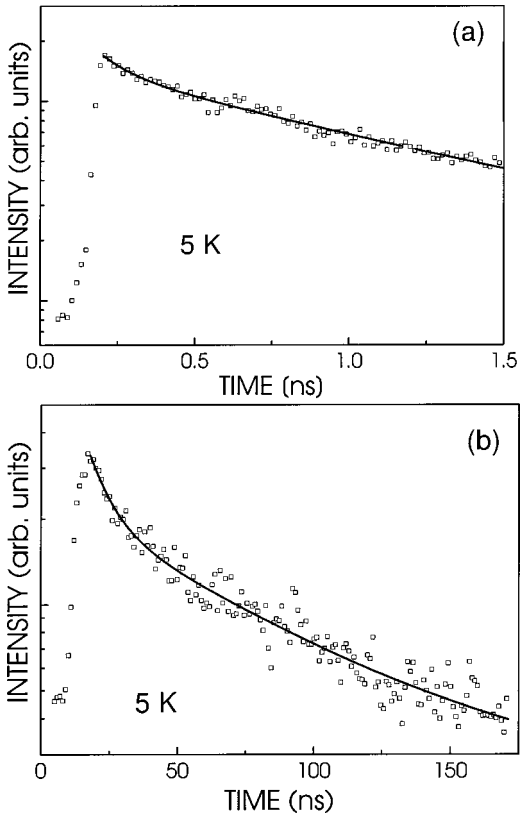

FIG. 11. PL transients of the SF emission from sample A (a) and the DAP transition from sample B (b) recorded at 5 K.

Figure 9 shows the spectrally integrated PL and CL intensities of both the *X* and DAP transitions versus the generation rate. Over five orders of magnitude, the intensity of the *X* transition rises linearly with an increase in excitation density. The *X* transition thus exhibits the characteristics expected for an intrinsic transition. In contrast, the DAP transition is saturated at generation rates exceeding 10^{19} cm^{-2} s^{-1}, confirming its extrinsic origin.

Although stacking faults do not introduce localized states in the band gap,[25] they form quantum-well-like structures since they can be considered to be thin zinc-blende layers embedded in the wurtzite matrix. The calculated band alignment[25–27] represents a type II heterojunction, where electrons are captured in the potential well, which then attract holes via Coulomb interaction and form excitons. Rebane *et al.*[26] also calculated the binding energy of these excitons to be 45 meV. In fact, in temperature-dependent PL measurements (not shown here) we found that the *X* emission quenches rapidly at elevated temperatures with an activation energy of 48 meV. The good agreement between these values, however, is likely to be a mere coincidence: the calculation of Rebane *et al.*[26] neglected the spontaneous polarization of the wurtzite matrix along the [0001] direction, i.e., perpendicular to the SFs.

Downloaded 18 Jun 2004 to 62.141.165.57. Redistribution subject to AIP license or copyright, see http://jap.aip.org/jap/copyright.jsp

Our TEM results show that the basal plane SFs terminated by Shockley-type partial dislocations are intrinsic type II SFs (also called I_2) with a stacking sequence *ABABABCACAC*,..., that contains two units of sphalerite stacking. Therefore, the width of the potential wells is given by $2c_0$, i.e., 1.04 nm. Figure 10 displays the band alignment of this type II SF within a wurtzite matrix obtained from self-consistent Schrödinger–Poisson calculations, taking the band offsets determined by Stampfl and van de Walle,[25] the spontaneous polarization given by Bernardini *et al.*,[28] and assuming that the SFs have spatial separation of 5 nm [cf. the SF bundle in Fig. 7(a)]. The band profile clearly shows that the electric field present in the barrier creates a triangular potential profile which effectively confines holes. The calculated interband transition energy agrees almost exactly with the experimental one, which, however, is somewhat fortuitous, since we did not take into account excitonic effects which would lower the transition energy by at least 30 meV.

Considering the band profile shown above, the recombination dynamics of the SF emission is expected to resemble that of quantum wells with similar width and magnitude of the electrostatic field. Figures 11(a) and 11(b) show the PL transients for the SF and DAP transitions, respectively. The measured decay time of the SF transition is 1.1 ns, which indeed is close to values reported for quantum wells of similar width.[29,30] In contrast, the decay of the DAP transition is nonexponential and takes place on a time scale of about 100 ns, showing the behavior expected for this extrinsic transition.

IV. SUMMARY

We have investigated the structural and optical properties of *M*-plane GaN$(1\bar{1}00)$ films grown on $LiAlO_2(100)$ with nucleation layers grown at high and low temperatures. High-temperature nucleation was demonstrated to give rise to the occurrence of bundles of SFs in the layers. The formation of these SFs is related to the thermal dissociation of the substrate, which triggers their formation by the generation of either steps or interfacial compounds. The SF bundles manifest themselves in a peculiar photoluminescence line at 3.356 eV, which may even dominate the spectrum at low temperature. We have shown that the nature of this emission line is intrinsic. This intrinsic transition is due to excitons bound to SFs and is consistent with considering that the SFs act as an ultrathin quantum well. Low-temperature nucleation was shown to be effective in reducing the SF density in the layers, and it is also a prerequisite for improving their surface morphology.

ACKNOWLEDGMENTS

The authors thank M. Ramsteiner for the Raman measurements, and M. Kästner for a critical reading of the manuscript.

[1] P. Waltereit, O. Brandt, A. Trampert, H. T. Grahn, J. Menniger, M. Ramsteiner, M. Reiche, and K. H. Ploog, Nature (London) **406**, 865 (2000).
[2] E. S. Hellman, Z. Liliental-Weber, and D. N. E. Buchanan, MRS Internet J. Nitride Semicond. Res. **2**, 30 (1997).
[3] B. Rau, P. Waltereit, O. Brandt, M. Ramsteiner, K. H. Ploog, J. Puls, and F. Henneberger, Appl. Phys. Lett. **77**, 3343 (2000).
[4] S. Ghosh, P. Waltereit, O. Brandt, H. T. Grahn, and K. H. Ploog, Appl. Phys. Lett. **80**, 413 (2002).
[5] S. J. Beckerman, R. B. Ford, and M. T. Nemeth, Powder Diffr. **11**, 312 (1996).
[6] B. Cockayne and B. Lent, J. Cryst. Growth **54**, 546 (1981).
[7] J. W. Lee, S. J. Pearton, C. R. Abernathy, R. G. Wilson, B. L. Chai, F. Ren, and J. M. Zavada, Mater. Res. Soc. Symp. Proc. **449**, 1041 (1997).
[8] A. Novoselov and A. Pajaczkowska, Cryst. Res. Technol. **6**, 949 (1998).
[9] B. J. Skromme, J. Jayapalan, R. P. Vaudo, and V. M. Phanse, Appl. Phys. Lett. **74**, 2358 (1999).
[10] K. Kornitzer, T. Ebner, K. Thonke, R. Sauer, C. Kirchner, V. Schwegler, M. Kamp, M. Leszczynski, I. Grzegory, and S. Porowski, Phys. Rev. B **60**, 1471 (1999).
[11] T. W. Kang, S. H. Park, H. Song, T. W. Kim, G. S. Yoon, and C. O. Kim, J. Appl. Phys. **84**, 2082 (1998).
[12] H. Teisseyre *et al.*, Phys. Rev. B **62**, 10151 (2000).
[13] S. O. Kucheyev, M. Toth, M. R. Phillips, J. S. Williams, and C. Jagadish, Appl. Phys. Lett. **79**, 2154 (2001).
[14] C. H. Hong, D. Pavlidis, S. W. Brown, and S. C. Rand, J. Appl. Phys. **77**, 1705 (1995).
[15] L. Eckey, A. Hoffmann, R. Heitz, I. Broser, B. K. Meyer, T. Detchprohm, K. Hiramatsu, H. Amano, and I. Akasaki, Mater. Res. Soc. Symp. Proc. **395**, 589 (1996).
[16] L. Eckey *et al.*, Appl. Phys. Lett. **68**, 415 (1996).
[17] C. Wetzel, S. Fischer, J. Krüger, E. E. Haller, R. J. Molnar, T. D. Moustakas, E. N. Mokhov, and P. G. Baranov, Appl. Phys. Lett. **68**, 2556 (1996).
[18] W. Rieger, R. Dimitrov, D. Brunner, E. Rohrer, O. Ambacher, and M. Stutzmann, Phys. Rev. B **54**, 17596 (1996).
[19] N. Grandjean, M. Leroux, M. Laügt, and J. Massies, Appl. Phys. Lett. **71**, 240 (1997).
[20] C. Trager-Cowan, S. McArthur, P. G. Middleton, K. P. O'Donnell, D. Zubia, and S. D. Hersee, Mater. Sci. Eng., B **59**, 235 (1999).
[21] T. Y. Liu, A. Trampert, Y. J. Sun, O. Brandt, and K. H. Ploog (unpublished).
[22] S. Hagege, S. Tanaka, and Y. Ishida, J. Phys. (France) **49**, 189 (1988).
[23] S. Hagege, S. Tanaka, and Y. Ishida, J. Jpn. Inst. Met. **52**, 1192 (1988).
[24] S. Hagege and Y. Ishida, Philos. Mag. A **63**, 241 (1991).
[25] C. Stampfl and C. G. V. de Walle, Phys. Rev. B **57**, 15052 (1998).
[26] Y. T. Rebane, Y. G. Shreter, and M. Albrecht, Phys. Status Solidi A **164**, 141 (1997).
[27] Z. Z. Bandic, T. C. McGill, and Z. Ikonic, Phys. Rev. B **56**, 3564 (1997).
[28] F. Bernardini, V. Fiorentini, and D. Vanderbilt, Phys. Rev. B **63**, 193201 (2001).
[29] P. Lefebvre *et al.*, Appl. Phys. Lett. **78**, 1252 (2001).
[30] M. S. Minsky, S. B. Fleischer, A. C. Abare, J. E. Bowers, E. L. Hu, S. Keller, and S. P. Denbaars, Appl. Phys. Lett. **72**, 1066 (1998).

Downloaded 18 Jun 2004 to 62.141.165.57. Redistribution subject to AIP license or copyright, see http://jap.aip.org/jap/copyright.jsp